AMERICAN JOURNAL OF PHYSICAL ANTHROPOLOGY 141:38–51 (2010)

Comparative 3D Quantitative Analyses of Trapeziometacarpal Joint Surface Curvatures Among Living Catarrhines and Fossil Hominins

M.W. Marzke,[1]* M.W. Tocheri,[2] B. Steinberg,[3] J.D. Femiani,[4] S.P. Reece,[5] R.L. Linscheid,[6] C.M. Orr,[1,7] and R.F. Marzke[8]

[1]*School of Human Evolution and Social Change, Arizona State University, Tempe, AZ 85287-2402*
[2]*Human Origins Program, Department of Anthropology, National Museum of Natural History, Smithsonian Institution, Washington DC 20013-7012*
[3]*Northwest Alliance for Computational Science and Engineering, Oregon State University, Corvallis, OR 97331-5501*
[4]*Division of Computing Studies, Arizona State University, Tempe, Arizona 85287-0180*
[5]*1836 NE Noble Avenue, Corvallis, Oregon 97330*
[6]*Mayo Clinic, Rochester, MN 55905*
[7]*Institute of Human Origins, Arizona State University, Tempe, AZ 85287-2402*
[8]*Department of Physics and Astronomy, Arizona State University, Tempe, AZ 85287-1504*

KEY WORDS thumb; morphology; stereophotogrammetry; laser scanning; geometric modeling

ABSTRACT Comparisons of joint surface curvature at the base of the thumb have long been made to discern differences among living and fossil primates in functional capabilities of the hand. However, the complex shape of this joint makes it difficult to quantify differences among taxa. The purpose of this study is to determine whether significant differences in curvature exist among selected catarrhine genera and to compare these genera with hominin[1] fossils in trapeziometacarpal curvature. Two 3D approaches are used to quantify curvatures of the trapezial and metacarpal joint surfaces: (1) stereophotogrammetry with nonuniform rational B-spline (NURBS) calculation of joint curvature to compare modern humans with captive chimpanzees and (2) laser scanning with a quadric-based calculation of curvature to compare modern humans and wild-caught *Pan*, *Gorilla*, *Pongo*, and *Papio*. Both approaches show that *Homo* has significantly lower curvature of the joint surfaces than does *Pan*. The second approach shows that *Gorilla* has significantly more curvature than modern humans, while *Pongo* overlaps with humans and African apes. The surfaces in *Papio* are more cylindrical and flatter than in *Homo*. *Australopithecus afarensis* resembles African apes more than modern humans in curvatures, whereas the *Homo habilis* trapezial metacarpal surface is flatter than in all genera except *Papio*. Neandertals fall at one end of the modern human range of variation, with smaller dorsovolar curvature. Modern human topography appears to be derived relative to great apes and *Australopithecus* and contributes to the distinctive human morphology that facilitates forceful precision and power gripping, fundamental to human manipulative activities. Am J Phys Anthropol 141:38–51, 2010.
© 2009 Wiley-Liss, Inc.

The perennial debate about the role of prehistoric tool use and tool making in the evolution of the human hand has focused especially on thumb morphology and, to a large extent, specifically on the joint at the base of the thumb between the trapezium and the first metacarpal, hereafter referred to as the trapeziometacarpal (tmc) joint. This focus is justified by the functional importance of an opposable thumb for manipulating objects with the hands. The articular surfaces of the tmc joint are typically saddle-shaped in humans and other catarrhines (Rose, 1992), facilitating opposition of the thumb pad to the pads of the fingers, a function compatible with one-handed manipulation of food and other objects.

Interest in fossil hominin tmc joint topography was stimulated by the discovery of hand bones (O.H. 7), along with other hominin elements, at Olduvai in 1960 (Leakey, 1960). These hand remains, which include a right trapezium, were described by Napier (1962) and subsequently were assigned as part of the type specimen of *Homo habilis* (Leakey et al., 1964). Napier (1962) described the O.H. 7 trapezium as having a saddle surface for the first metacarpal. Lewis (1977, 1989) noted that this surface recalls the human one in having a broader dorsovolar extent than in chimpanzees, although he observed that some gorilla specimens also share this

[1]The term "hominin" refers to members of the tribe Hominini, which includes modern humans and fossil species that are related more closely to modern humans than to extant species of chimpanzees, Wood and Lonergan (2008). Hominins are in the family Hominidae with great apes.

Grant sponsor: National Science Foundation; Grant number: IIS 998016; Grant sponsor: National Institutes of Health, Division of Research Resources; Grant number: U42RR15090-01; Grant sponsors: The Smithsonian Institution Fellowship Program, The ASU College of Liberal Arts and Sciences.

*Correspondence to: Mary W. Marzke, School of Human Evolution and Social Change, Arizona State University, Tempe, AZ 85287-2402. E-mail: mary.marzke@asu.edu

Received 11 November 2008; accepted 7 May 2009

DOI 10.1002/ajpa.21112
Published online 19 June 2009 in Wiley InterScience (www.interscience.wiley.com).

© 2009 WILEY-LISS, INC.

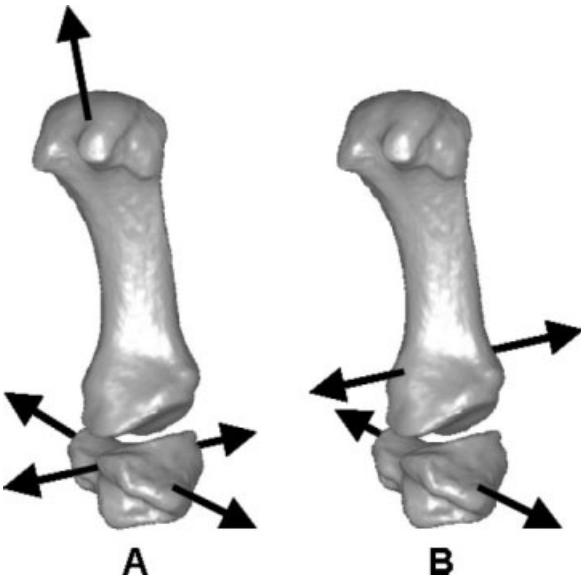

Fig. 1. Trapeziometacarpal joint axes of motion after (**A**) Napier (1955) and (**B**) after Hollister et al. (1992). Note that in contrast to (B) the flexion/extension and abduction/adduction axes of (A) are perpendicular to one another and in the same plane, and a longitudinal axis is assumed for metacarpal axial rotation at mid-position on the trapezium.

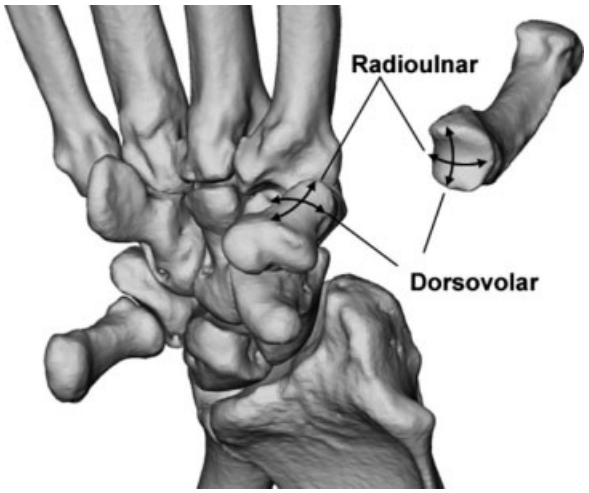

Fig. 2. Dorsovolar and radioulnar curvature directions of the trapeziometacarpal joint surfaces on the trapezium and first metacarpal. The "set" of the trapezium within the wrist varies between individuals and taxa; therefore, in a comparative context, the radioulnar axis will not always be consistently oriented relative to the radius and ulna. However, in this work, we use the term *radioulnar* by convention. The dorsal aspect of the bone is fixed by developmental homology.

feature. Susman and Creel (1979, p. 329) considered the surface to be "very human in appearance." Day (1978) inferred from the surface morphology a facility for a wide range of thumb movements associated with both power and precision thumb postures (including rotation).

Trinkaus (1989) conducted the first quantitative study of the articular morphology of this joint in modern humans, Neandertals, and O.H. 7. He quantified the curvature of the trapezial facet for the thumb metacarpal using caliper chord and subtense measurements and found that the O.H. 7 surface is significantly flatter than those of modern humans. His measured radioulnar curvature of the surface in O.H. 7 is between one and two SD below the mean for his modern human sample, and at the lower limit of the modern human range. The mean dorsovolar curvature is more than two SD below the recent human mean, lying outside the range altogether. Similar dorsovolar flatness was also found in his sample of Neandertals. His functional inferences from this topography were that axial pronation may have been enhanced by the relatively flat first metacarpal saddle surface on the trapezium, and large axial joint reaction forces could have been accommodated by the surface.

TRAPEZIOMETACARPAL JOINT MOTION, STRENGTH AND STABILITY

Formulating hypotheses about the functional implications of variability among genera in joint surface curvature requires data on joint motion, strength, and stability in living species (Hamrick, 1996). The following review of studies on human and nonhuman catarrhine genera reveals a limited knowledge base, but one that can be applied to general predictions of functional variability from morphological variability.

Joint motion

The human tmc saddle joint has two degrees of freedom (movement around a flexion/extension axis and around an abduction/adduction axis) (see Fig. 1), but conjunct motion about these axes produces pronation/supination (Cooney et al., 1981). That is, pronation of the metacarpal during opposition of the thumb to the fingers is a function of combined rotation about the flexion/extension axis (in the trapezium) and the abduction/adduction axis (in the metacarpal base) (Hollister et al., 1992). Because these axes are not perpendicular to one another or to the bones and are offset from the anatomical planes (Hollister et al., 1992; Brand and Hollister, 1999), the metacarpal comes into a position of opposition to the remaining metacarpals as flexion and abduction occur, with the amount of pronation fixed by the degrees of flexion and abduction (Hollister et al., 1992) (see Fig. 2). Validation of this kinematic model of tmc movements by an in vivo analysis using an optoelectronic system has been reported recently by Cerveri et al. (2008).

Relative motion of the mutual tmc joint surfaces has been found to occur by sliding rather than by rolling (Napier, 1955; Pieron, 1973; Martin et al., 1998). In vivo measurements of active motion at the human tmc joint were made by Cooney et al. (1981) using biplanar X-rays. The metacarpal moved through a median flexion/extension range of 53° and abduction/adduction range of 42°. The accompanying pronation/supination was 17°. Rose (1992) obtained comparable measurements for human metacarpal abduction/adduction (46.3°) using a goniometer to record thumb metacarpal bone movement relative to the trapezium in a skeletal collection. However, his measurement of flexion/extension range (47.6°) was substantially lower than the range reported by Cooney et al. (1981). Using the same approach for great apes, Rose (1992) found mean flexion/extention of 32.8° and abduction/adduction of 34.9°, both lower than in his human sample. Cercopithecine ranges were still lower,

with 21.4° flexion/extension and 18.1° abduction/adduction.

Unfortunately, until more sophisticated studies are made of nonhuman catarrhine tmc movement capabilities, estimates of differences among catarrhine genera will remain primarily qualitative and based upon comparative topography of the joint surfaces. However, it does seem reasonable to conclude from Rose's (1992) measurements that overall the ranges of motion will prove to be lower in great apes and *Papio* than in modern humans.

Joint strength

A classic 3D study of static forces in the thumb revealed that for an applied load of 1 kg by the thumb and index finger during pinch, the tmc joint contact load averages 12 kg (Cooney and Chao, 1977). For an applied load of 10 kg in grasp (with the thumb opposing all the fingers), average tmc joint contact load is 120 kg (ibid.). Accommodation of these loads depends upon the extent to which orientation of the surfaces is normal to the axial loads (Sarmiento, 1988; Hamrick, 1996) and the degree of joint surface congruence in various grips. Measurements of joint contact areas in humans have been made in vitro for grasp, in which the thumb metacarpal is flexed, abducted, and pronated to oppose the four fingers, and for the lateral pinch posture, in which the metacarpal is held against the side of the index finger in adduction-flexion. Momose et al. (1999) found that contact area was largest in opposition, with 53% of the mutual trapezium and first metacarpal surfaces in contact. During lateral pinch, contact is in the palmar compartment of the joint (Pellegrini, 2005).

Ateshian et al. (1992) and Xu et al. (1998) found that the human female tmc joint is less congruent than in males and concluded that joint contact areas in females are smaller than in males and thus subject to greater stress. They consider that this difference may be a factor in the higher occurrence of degenerative joint disease in females.

The finding by Guthrie (1991) of a larger radius of curvature of the tmc surfaces in humans compared with chimpanzees indicates that a proportionately larger surface of the human joints is normal to axial loads. Measurements of joint contact have not been made in nonhuman catarrhines, but behavioral observations of chimpanzee and Hamadryas baboon manipulative behavior indicate that maximum axial loading of the joint is lower in these genera (Guthrie, 1991; Jude, 1993; Marzke and Wullstein, 1996).

Joint stability

Stability of a joint is associated with its capacity to resist displacement in a given direction (Hamrick, 1996). Relatively large joint surface contact areas in grasp (Momose et al., 1999) contribute to stability of the human joint. However, there is less joint surface contact and a tendency for the metacarpal to sublux dorsally during pinch by the thumb and index finger (Eaton and Dray, 1982). Thus stability is dependent primarily upon ligaments (Bettinger et al., 1999, 2000; Bettinger and Berger, 2001; Pellegrini, 2005; Colman et al., 2007; Leversedge, 2008) It is suspected that laxity of the tmc ligaments, particularly, the deep anterior oblique or beak ligament (Pellegrini et al., 1993; Pellegrini, 2001), and the dorsoradial ligament (Bettinger et al., 2000; Colman et al., 2007) can lead to incongruent loading of the trapezial and metacarpal surfaces and to shear forces, as the unstable metacarpal slides and damages the articular cartilage (Ateshian et al., 1994, 1995; Imaeda et al., 1994; Bettinger et al., 2000; Pellegrini, 2005; Koff et al., 2006; Colman et al., 2007).

GOALS OF THE STUDY

The purpose of the study is to first determine whether significant differences in tmc joint curvature exist among five extant catarrhine genera (*Homo*, *Pan*, *Gorilla*, *Pongo*, and *Papio*), and then to compare these data with those of various hominin fossils.

To reliably compare living and fossil primates in tmc joint shape and to make reasonable functional interpretations, metrics that accurately describe the curvatures at this joint in 3D are required. In this study, we use two 3D approaches to quantify and compare the curvatures of the mutual trapezial and first metacarpal joint surfaces. The first approach used stereophotogrammetry with B-spline surface analysis and was applied to a small sample of humans and chimpanzees while the second used laser scanning with quadric surface analysis, and was applied to a much larger catarrhine sample in order to broaden the comparative scope of the study and increase the statistical power of the results. It was equally important to determine whether the two quantitative approaches lead to similar results, because they involve different and complex steps in the estimate of joint surface curvature.

The present study quantitatively tests a null hypothesis of shape equivalence in tmc joint curvature among these five extant catarrhine genera, and several fossil hominin taxa are examined against this background. Based upon previous studies in the literature, our own qualitative observations of this joint in living and fossil primates, and current understanding of functional correlates to structural variability, we made the following predictions (all of which, we note, violate the null hypothesis to a greater or lesser extent):

1. The mutual surfaces at the tmc joint in modern humans should have less curvature than in African apes and *Pongo*, but more curvature than in *Papio*. If true, then this suggests that the modern human joint topography is most parsimoniously interpreted as derived from a more curved condition like that observed in the great apes. Furthermore, this would suggest that the human joint is less stable, joint contact areas are primarily in the transverse plane (normal to axial loads), and tmc stability is more dependent upon ligament constraints.
2. Neandertals should have joint surface curvatures more similar to modern humans than to the great apes, but with relatively less curvature dorsovolarly than in modern humans (Trinkaus, 1989). This would suggest an ability to accommodate large axial loads on the joint associated with muscle contraction during strong pinch and grasp, but it also indicates possible instability of the joint because of the lack of skeletal constraints on dorsal sliding of the metacarpal on the trapezium during pinch.
3. The O.H. 7 trapezium should show less curvature dorsovolarly and radioulnarly than in modern humans, but similar dorsovolar curvature to Neandertals (Trinkaus, 1989). This would suggest an unstable joint prone to subluxation but capable of withstanding large axial loads.

TABLE 1. Comparative samples

Genus	Trapezia	Metacarpals	Human population	Trapezia	Metacarpals
SPG APPROACH					
Homo	58	58	Aleut	8	8
			South Dakota Native American	13	13
			Chinese	9	9
			African American	14	14
			Euro-American	14	14
Pan	13	13			
LS APPROACH					
Homo	113	121	Aleut and Pre-Aleut	11	15
			South Dakota Native American	8	9
			Chinese	23	25
			African Bantu	4	4
			Australian Aborigine	7	9
			African American	30	29
			Euro-American	*30*	*30*
Pan	47	46			
Gorilla	44	47			
Pongo	21	19			
Papio	20	19			

FOSSILS

Species	Trapezia	Metacarpals
Australopithecus afarensis	A.L. 333-80	A.L. 333-58
		A.L. 333w-39
Paranthropus robustus?	O.H. 7	SK 84
Homo habilis		
Homo sp.?		SKX 5020
Homo neanderthalensis	Kebara 2	Kebara 2
	La Ferrassie 1	La Ferrassie 1
	La Ferrassie 2	La Ferrassie 2
	Regourdou 1	Regourdou 1
		Amud 1
		La Chapelle-aux-Saints 1
	Shanidar 3	
	Shanidar 4	

4. The *A. afarensis* trapezium and first metacarpals should be more similar to those of African apes than humans in surface curvature (Guthrie, 1991). This would indicate a joint that was stable in pinch grips against dorsal sliding of the metacarpal. Proportionately less of the mutual joint surfaces would be oriented normal to axial loads.
5. Thumb metacarpals from Swartkrans (SK 84 and SKX 5020) will differ in joint surface curvature, judging by differences between them in other aspects of morphology described by Susman (1988a,b).

These predictions were tested in three stages. First, the topography of the mutual trapezial and first metacarpal joint surfaces was quantified, using the two previously mentioned approaches to 3D data acquisition and analysis. Second, comparative statistical analyses of the 3D topography in the extant sample were performed. Finally, the distribution of fossil hominin trapezial and first metacarpal joint surface curvatures was examined relative to those of the extant comparative sample.

MATERIALS AND METHODS

Stereophotogrammetry approach

Fifty-eight trapezia and 58 first metacarpals from five human groups were photographed at the Smithsonian Institution's National Museum of Natural History (NMNH) (Table 1). The groups represented were Aleuts, South Dakota Native Americans, Chinese, from a group of immigrant workers in Alaska, and African Americans, and Euro-Americans from the Terry Collection. Mutual trapezial and first metacarpal joint surface images were also obtained for 13 individuals in the Primate Foundation of Arizona chimpanzee skeletal collection and for casts of bones from *A. afarensis* (A.L. 333-80, trapezium; A.L. 333w-39, first metacarpal) and *H. habilis* (O.H. 7, trapezium). Each joint surface was examined for evidence of osteoarthritis. Criteria used in judging this included signs of eburnation and osteophyte development. No pathology was found in the chimpanzee specimens, and only minor signs of osteoarthritis were found in seven of the human joint surfaces.

Images of the mutual trapezial and first metacarpal joint surfaces were obtained following methods similar to those of Ateshian et al. (1992). A Pixera digital camera was used, operated with software run from a standard PC (Pixera Camera Suite model 120 es camera, version 2.5). This camera took the place of the large format photographic Sinar film cameras used by Ateshian et al. (1992). The mutual joint surfaces were photographed together in pairs, in most cases, each bone being positioned on clay in a plastic (Delrin) frame with a circular front opening 1.5 in. in diameter. Calibration markers were inserted into the front face of the frame at fixed positions surrounding the opening, providing both a length scale and an accuracy check for the 3D stereophotogrammetric joint surface digitizing procedure. A grid of intersecting lines was projected onto the joint surfaces,

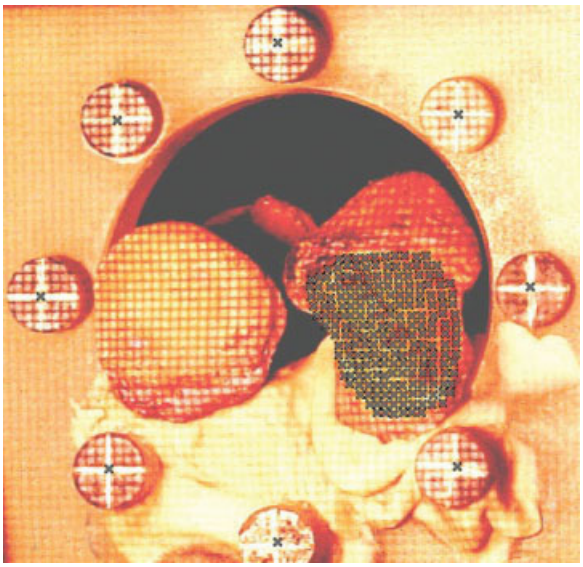

Fig. 3. Photograph of mutual human metacarpal and trapezial joint surfaces, mounted on clay in a calibration frame (a color version of this figure can be found in the on-line version). A grid is projected onto the surfaces, and the intersections of its lines provide points that are shown digitized on the trapezium at the right. [Color figure can be viewed in the online issue, which is available at www.interscience.wiley.com.]

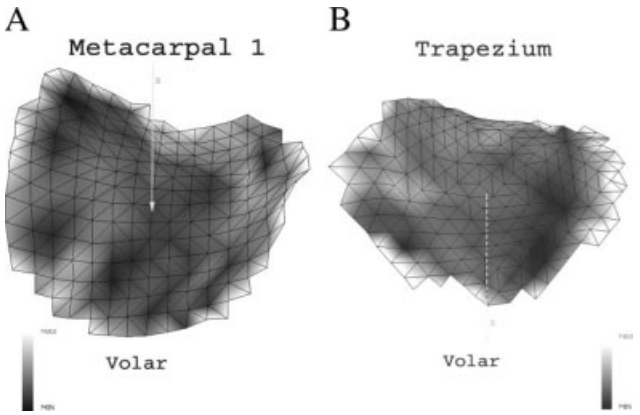

Fig. 4. RMS curvature maps of mutual joint surfaces on a human first metacarpal and trapezium from the right hand, viewed along the long (z) axis of the metacarpal. Gradations from black to white reflect the range from lower to higher curvature.

using a standard slide projector and a 35-mm slide made by photographing an accurately drawn rectangular grid (see Fig. 3). Three digital photographs were then taken, along three directions with respect to an axis approximately normal to the frame's front facial plane. The camera angles used were $\sim 30^\circ$ to the left of this normal axis, 30° to the right, and along the axis itself. Digitizing and 3D modeling of the three photographs for each surface was done using Photomodeler software (EOS Systems, Vancouver, B.C.). This approach produced accurate results, with digitizing errors rarely exceeding 0.5%.

The datasets obtained from Photomodeler, consisting of 100 or more digitized points in 3D, were exported to a C^{++} program (Steinberg, 1999), which fitted each dataset to NURBS (nonuniform rational B-spline) functions. For this purpose, a subset of points representing the boundary of each joint surface had to be separately digitized, from the original photographs. Generation of each boundary point set for a surface was straightforward, using the original images that had been previously marked for the full surface's stereophotogrammetry.

The NURBS program calculated total surface area and point-by-point root mean square (RMS) curvature. This curvature is considered by Ateshian et al. (1992) to provide the most unambiguous quantitative index of overall flatness of a surface. It is defined in Eq. (4) below and is the inverse of a radius of curvature. The effects of overall joint size on curvature values were normalized following the procedure of Ateshian et al. (1992), dividing the radius of curvature for each joint by a radius representing its effective size, namely the square root of the joint surface area. Figure 4 shows an example of a grayscale display of the RMS curvatures of mutual metacarpal and trapezial surfaces. Regions of lowest RMS curvature are solidly filled and those with highest curvature are lightly filled. Finally, normalized RMS curvature values were averaged over each metacarpal and trapezium surface, leading to a single average value for curvature of each surface as a whole.

Statistical analyses of the significance of the observed differences between groups, particularly in average normalized RMS curvatures, were performed using standard two-sample resampling or randomization testing techniques (Simon, 1974–1997; Mooney and Duval, 1993; Bruce et al., 1997; Edgington, 1995).

Laser scanning approach

Joint surfaces on 252 metacarpals and 249 trapezia of five extant catarrhine genera from the NMNH and the Cleveland Museum of Natural History were examined (Table 1). *Pan* is represented by a sample of *P. troglodytes*, *Gorilla* by *G. gorilla* and *G. beringei*, and *Pongo* by *P. pygmaeus* and *P. abelii*. *Papio* is represented by a combined sample of *P. anubis*, *P. cynocephalus*, *P. hamadryas*, and *P. ursinus*. The sample of *H. sapiens* includes individuals of several populations. The fossil specimens (Table 1) were all casts, with the exception of Shanidar 3. Joint surface pathology or osteoarthritis was minimal throughout the laser scanned sample.

All bones were scanned using the Cyberware Model 15 desktop laser digitizer. Each 3D model is a high-resolution triangular mesh consisting on average of more than 1,000 points per square centimeter. The mesh of each 3D model was digitally segmented into articular and nonarticular areas using commercial software. In most cases, individual articular areas were segmented while referring visually to the actual bone. Following segmentation, curvatures were calculated by fitting modeled quadric surfaces to the segmented joint surfaces (Christie and Ridley, 1990; Tocheri et al., 2006; Tocheri, 2007; Tocheri and Femiani, in press). In 3D, a quadratic surface has the following equation:

$$z = ax^2 + by^2 + 2cxy + 2dx + 2ey + f. \quad (1)$$

If the following rigid body transform is used,

$$\begin{bmatrix} \hat{x} \\ \hat{y} \\ \hat{z} \end{bmatrix} = R \begin{bmatrix} x - x_0 \\ y - y_0 \\ z - z_0 \end{bmatrix} \quad (2)$$

where R is a 3 × 3 matrix with elements expressed in terms of the constants $a \ldots f$, the surface's equation may be put into the following quadric form:

$$\hat{z} = A\hat{x}^2 + B\hat{y}^2 \quad (3)$$

where A and B summarize the shape of the surface and are functions of the parameters a through f. The A and B coefficients determine the principal curvatures (k_{max} and k_{min}) of the fitted quadric surface along the principal directions at the origin of x, y, z space. Thus, $A = k_{max}$ and $B = k_{min}$. Figure 5 gives an example of a surface that has a quadric shape given by (3), with $A = -B$. This trapeziumlike surface has a convex curve in the y (flexion/extension or dorsovolar) direction and a concave curve in the x (abduction/adduction or radioulnar) direction. Figure 6 shows the shapes of the quadric surfaces generated by varying signs and magnitudes of A and B. If A and B have the same sign, the surface is of an elliptical or parabolic form, whereas if A and B are different in sign, the surface is of hyperbolic or saddle form. The relative magnitudes of A and B thus reflect the degree of curvature in each of the principal coordinates of the surface. The effects of overall joint size on A and B were normalized by the square root of the joint surface area. These normalized A and B values were used to calculate the RMS curvature of the fitted surface, where this curvature is defined as

$$k_{RMS} = \sqrt{(k_{max}^2 + k_{min}^2)/2} \quad (4)$$

As noted in the previous section on SPG, RMS curvature provides what Ateshian et al. (1992) consider to be "an unambiguous quantitative index of flatness." A and B were also used to calculate absolute, Gaussian, and mean surface curvatures. These are defined as follows:

Absolute curvature (k_{abs}):

$$K_{abs} = |k_{min}| + |k_{max}| \quad (5)$$

Gaussian curvature (k_{gauss}):

$$K_{gauss} = k_{min} \times k_{max} \quad (6)$$

Mean curvature (k_{mean}):

$$K_{mean} = (k_{min} + k_{max}) \quad (7)$$

In all cases, it was assumed that the curvatures in the surface along the principal directions reasonably approximate the curvatures in the dorsovolar (flexion/extension) and radioulnar (abduction/adduction) directions, thus giving numerical values for these two directions.

Numerical measures of the degree of congruence of surfaces (e.g., metacarpal and trapezial) in (near) contact with one another have been developed from differential geometry and were applied to our data, following the approach of Ateshian et al. (1992) to his sample of human tmc joints. These measures are based upon maximum and minimum curvatures k_{max} and k_{min}. The basic approach consists of introducing a surface that effectively represents the difference between any two surfaces in contact at a point, that is, a surface whose numerical values, when added to the lower of the two surfaces, yield the upper one. This difference surface, called the effective surface, is represented as a curved surface in contact with a plane, and its maximum and minimum curvatures, denoted as k_{max}^e and k_{min}^e, are called congruence indices. Their use is appropriate, because for surfaces that are perfectly congruent the effective surface is

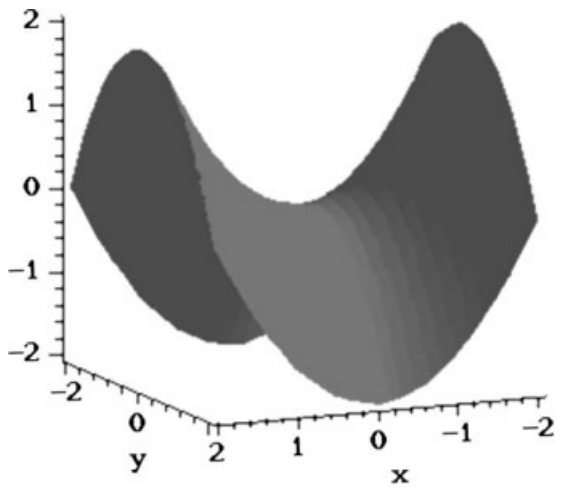

Fig. 5. Example of a surface that has a quadric shape given by (3), with $A = -B$.

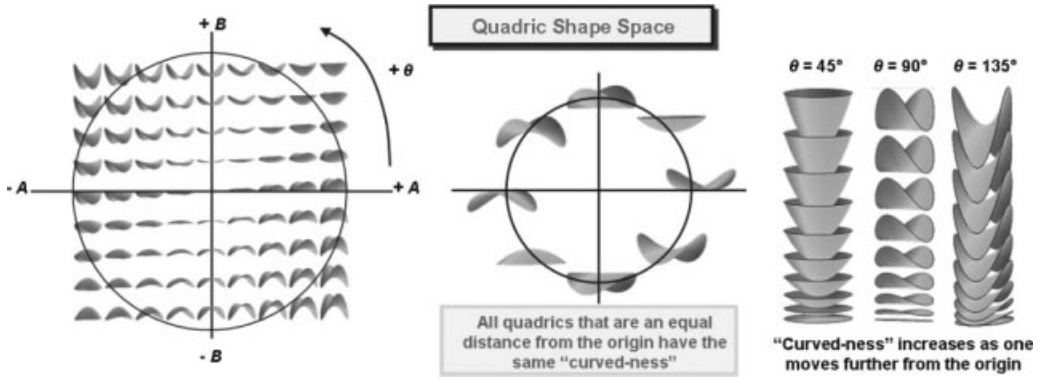

Fig. 6. Shapes of the quadric surfaces generated by varying signs and magnitudes of A and B (left). All quadric surfaces that are equidistant from the origin have the same amount of curvature (middle), which increases as one moves further from the origin (right).

a plane, and its principal curvatures vanish. Also, the less congruent the surfaces, the larger the equivalent surface curvatures. Thus lower indices describe joint surface pairs that are more congruent than those with higher indices. Formulae for the equivalent surface curvatures in terms of the separate curvatures of the two surfaces in contact are given by Ateshian et al. (1992). For our study, we applied these formulae to normalized curvatures.

Statistical analyses of the observed curvature differences between groups were performed using the bootstrap (Efron and Tibshirani, 1993; Manly, 1997). With 20 pairwise comparisons for each curvature variable, a standard Bonferroni correction was applied to evaluate the statistical significance of each comparison ($P < 0.0025$ (0.05/20)). Differences in congruence index were analyzed with two-tailed *t*-tests.

In the text, tables and figures regarding tmc joint surfaces, "metacarpal" ("met") refers to the surface on the metacarpal for the trapezium and "trapezial" ("trap") refers to the surface on the trapezium for the metacarpal.

RESULTS

Comparison of *Pan* and *Homo* (SPG and LS approaches)

The results from both approaches show that, as predicted, the human mean RMS curvature of the metacarpal surface is significantly lower than the chimpanzee mean (Table 2). Significant differences in curvatures along the dorsovolar and radioulnar directions parallel the RMS surface curvature difference (Table 3).

SPG and LS RMS curvatures of the trapezial surface vary significantly among species in the same manner as for metacarpal surface curvatures (Table 2), as does the LS dorsovolar curvature (Table 3). However, humans and chimpanzees are not significantly different in trapezial surface radioulnar curvature (Table 3).

TABLE 2. Normalized mean joint surface RMS curvature values: significant differences in Homo and Pan

Genus	Approach	Joint surface	*N*	RMS curvature	SD	*P*
Homo	SPG	Metacarpal	58	1.25	0.18	<0.000
Pan			13	1.62	0.38	
Homo	SPG	Trapezium	58	1.37	0.29	<0.004
Pan			13	1.85	0.72	
Homo	LS	Metacarpal	121	0.93	0.13	<0.001
Pan			46	1.29	0.14	
Homo	LS	Trapezium	113	0.96	0.19	<0.001
Pan			47	1.41	0.25	

Comparisons among the extant genera (LS approach)

Pairwise comparisons of genus means for normalized dorsovolar, radioulnar, RMS, absolute, Gaussian, and mean curvature of the first metacarpal and trapezial surfaces are given in Table 3. Table 4 summarizes the rankings of genera in these curvature means. Bivariate plots show the relation between dorsovolar and radioulnar curvatures (Figs. 7 and 8), RMS and mean curvatures (Figs. 9 and 10), and absolute and mean curvatures for the metacarpal and trapezium surfaces (Figs. 11 and 12).

In all genera, the metacarpal is less curved than the trapezium in the dorsovolar direction and more curved than the trapezium in the radioulnar direction. At the proximal surface of the first metacarpal, the African apes are characterized by marked RMS curvature, whereas *Papio* is characterized by a much flatter surface (Fig. 9; Table 3). *Homo* falls between these two extremes, with significantly less RMS curvature than the African apes but significantly more than *Papio*. This pattern of differences is the same in dorsovolar curvature. Particularly striking are the marked RMS and dorsovolar curvatures in *Gorilla* compared with all the other genera. Radioulnar curvature is greatest in the great apes and least in *Papio*, *Homo* falling between with significant differences from both groups (Table 4).

The surface on the trapezium parallels that on the metacarpal closely, with RMS curvature high in the African apes, low in *Papio*, and intermediate in *Homo* (Fig. 10; Table 3). There are significant differences in all pairwise comparisons, except the one between *Pan* and *Gorilla*. Dorsovolar curvature follows the same distribution as RMS curvature (see Fig. 8), with the exception that the difference between *Homo* and *Papio* is smaller and not significant (Table 3). In radioulnar curvature, the

TABLE 4. Ranking of genera in descending order of mean curvatures

Dorsopalmar	Radioulnar	RMS	Absolute	Gaussian	Mean
Metacacarpal					
Gorilla	*Pongo*	*Gorilla*	*Gorilla*	*Gorilla*	*Pongo*
Pan	*Pan*	*Pan*	*Pan*	*Pan*	*Pan*
Pongo	*Gorilla*	*Pongo*	*Pongo*	*Pongo*	*Papio*/*Homo*
Homo	*Homo*	*Homo*	*Homo*	*Homo*	*Gorilla*
Papio	*Papio*	*Papio*	*Papio*	*Papio*	
Trapezium					
Gorilla	*Pongo*	*Gorilla*	*Gorilla*	*Gorilla*	*Gorilla*
Pan	*Homo*	*Pan*	*Pan*	*Pan*	*Pan*
Pongo	*Pan*/*Gorilla*	*Pongo*	*Pongo*	*Pongo*	*Papio*
Homo	*Papio*	*Homo*	*Homo*	*Homo*	*Pongo*
Papio		Papio	Papio	Papio	Homo

TABLE 3. Pairwise comparisons of normalized genus mean curvatures[1]

	Dorsovolar curvature		Radioulnar curvature		RMS curvature		Absolute curvature		Gaussian curvature		Mean curvature	
Genus	Met.	Trap.	Met.	Trap.	Met.	Trap.	Met.	Trap.	Met.	Trap.	Met.	Trap.
a. *Homo*	$0.39^{b,c,e}$	$-0.83^{b,c}$	-0.82^{ALL}	0.43^{e}	0.93^{ALL}	0.96^{ALL}	1.22^{ALL}	$1.27^{b,c,e}$	$-0.31^{b,c,e}$	$-0.35^{b,c,e}$	$-0.21^{b,c,d}$	$-0.20^{b,c,e}$
b. *Pan*	$0.52^{a,c,e}$	$-1.32^{a,d,e}$	$-1.14^{a,e}$	0.41^{e}	$1.29^{a,c,e}$	$1.41^{a,d,e}$	$1.69^{a,c,e}$	$1.75^{a,d,e}$	$-0.58^{a,c,e}$	$-0.52^{a,e}$	$-0.31^{a,c,e}$	$-0.46^{a,d}$
c. *Gorilla*	0.94^{ALL}	$-1.37^{a,d,e}$	$-1.11^{a,e}$	0.41^{e}	1.47^{ALL}	$1.45^{a,d,e}$	2.05^{ALL}	$1.45^{a,d,e}$	-1.04^{ALL}	$-0.56^{a,e}$	-0.09^{ALL}	$-0.48^{a,d,e}$
d. *Pongo*	$0.45^{c,e}$	$-0.98^{b,c,e}$	$-1.15^{a,e}$	0.44^{e}	$1.26^{a,c,e}$	1.11^{ALL}	$1.61^{a,c,e}$	$1.42^{b,c,e}$	$-0.52^{c,e}$	-0.40^{e}	$-0.35^{a,c,e}$	$-0.27^{b,c}$
e. *Papio*	0.22^{ALL}	$-0.78^{b,c,d}$	-0.64^{ALL}	0.10^{ALL}	0.68^{ALL}	0.80^{ALL}	0.86^{ALL}	0.90^{ALL}	-0.14^{ALL}	-0.07^{ALL}	$-0.21^{b,c,d}$	$-0.34^{a,c}$

[1] Superscripts indicate significant curvature differences among genera a–e at $\alpha < 0.0025$.

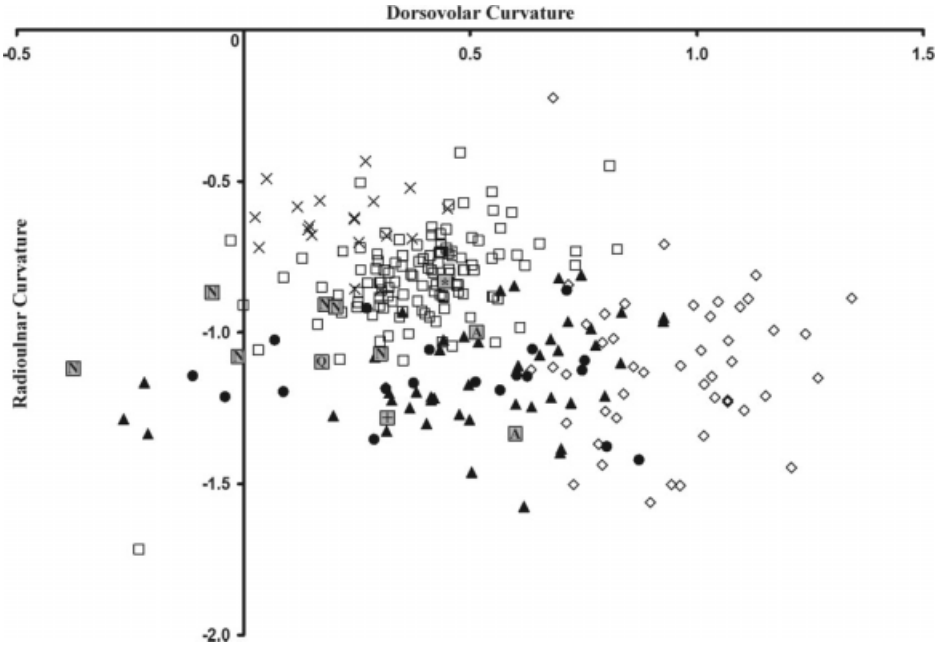

Fig. 7. Bivariate plot showing the relation between dorsovolar and radioulnar curvatures of the surface on the metacarpal (modern humans, open squares; *Pan*, closed triangles; *Gorilla*, open diamonds; *Pongo*, closed circles; *Papio*, X's; Neandertals, gray N's; *Australopithecus*, A's; SK 84, +; SKX 5020, *). Specimens closer to the origin exhibit less curvature than those further from the origin along each axis.

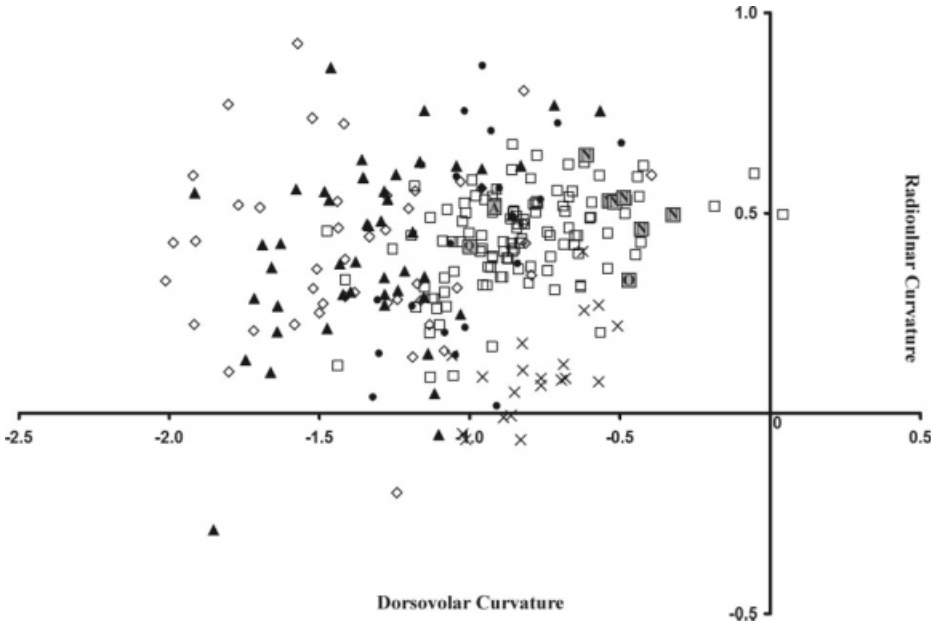

Fig. 8. Bivariate plot showing the relation between dorsovolar and radioulnar curvatures of the surface on the trapezium (modern humans, open squares; *Pan*, closed triangles; *Gorilla*, open diamonds; *Pongo*, closed circles; *Papio*, X's; Neandertals, gray N's; *Australopithecus*, A; O.H. 7, O). Specimens closer to the origin exhibit less curvature than those further from the origin along each axis.

trapezium departs from the metacarpal in exhibiting similar values among the great apes and humans (Fig. 8; Table 3). However, as in the metacarpal, each of these genera has significantly higher radioulnar curvature values than *Papio* (Table 3).

Both surfaces are significantly more curved in *Pongo* than in *Papio*, but otherwise *Pongo* does not consistently parallel either the African apes or humans. The metacarpal surface for the trapezium is similar to that of *Pan* in RMS and to the *Homo* surface in dorsovolar curvature, while radioulnar curvature falls with *Pan* and *Gorilla*, significantly above *Homo*. RMS and dorsovolar curvature of the trapezial surface are intermediate between the African apes and humans (and significantly different

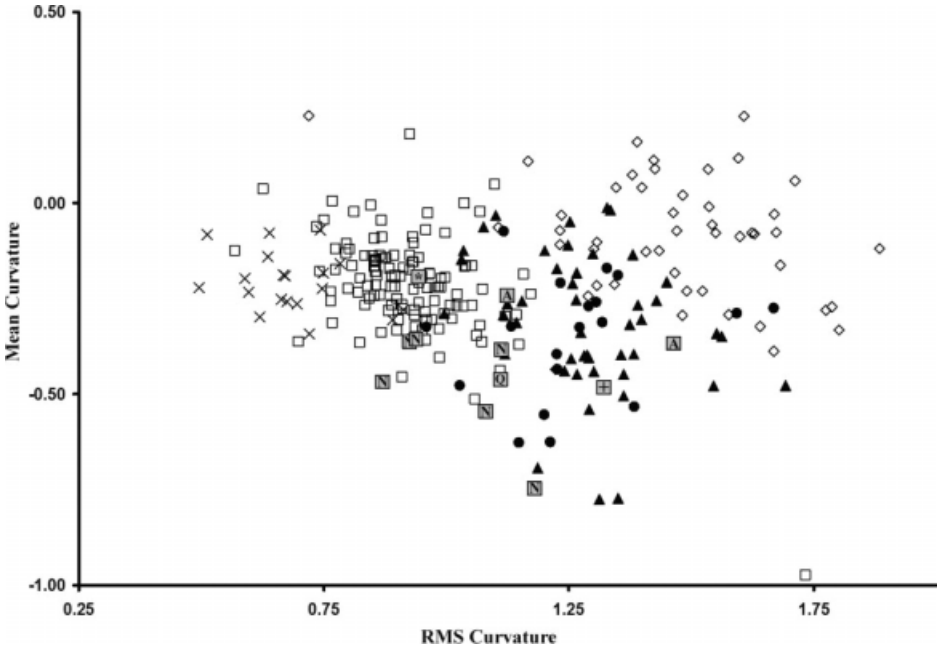

Fig. 9. Bivariate plot showing the relation between RMS and mean curvatures of the surface on the metacarpal (symbols as in Fig. 7). Greater values of RMS curvature indicate greater overall surface curvature; mean curvature values closer to zero indicate more evenly curved surfaces while negative values indicate radioulnar curvature is greater than dorsovolar curvature (and vice versa).

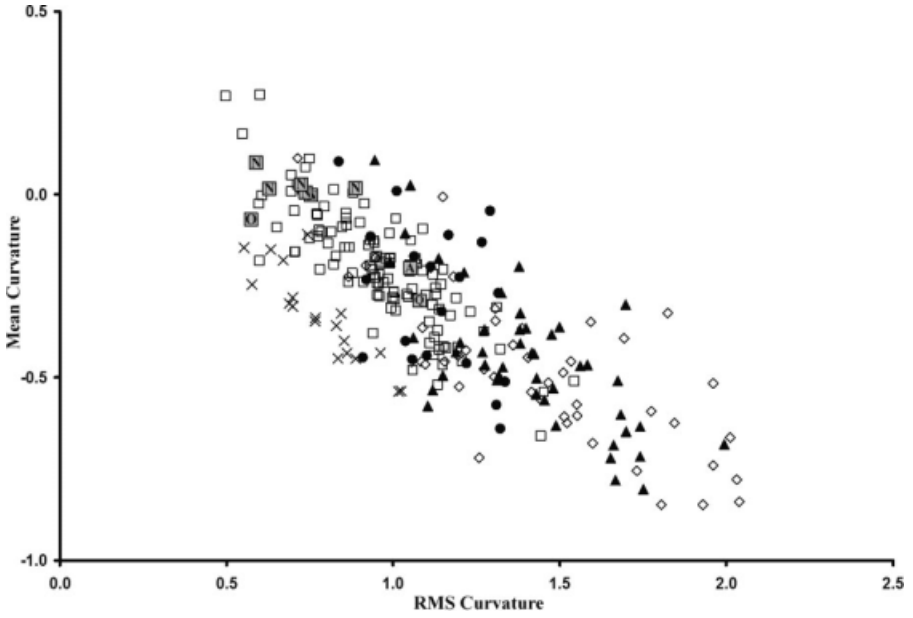

Fig. 10. Bivariate plot showing the relation between RMS and mean curvatures of the surface on the trapezium (symbols as in Fig. 8). Greater values of RMS curvature indicate greater overall surface curvature; mean curvature values closer to zero indicate more evenly curved surfaces while negative values indicate dorsovolar curvature is greater than radioulnar curvature (and vice versa).

except for *Homo*/*Pongo* dorsovolar), whereas radioulnar curvature falls close to the *Pan, Gorilla*, and *Homo* means.

Genus rankings of metacarpal and trapezium absolute curvature values are the same as for RMS curvature (Table 4). This is not surprising, because both measures reflect relative curvature magnitudes. Gaussian curvature, which reflects overall surface shape, shows again the same ranking in both surfaces. However, there are differences in rankings for mean curvature of both the metacarpal and trapezium surfaces. For saddle surfaces, mean curvature reflects the extent to which the principal curvatures differ from one another in magnitude: the more similar the principal curvatures are to one another, the lower the mean curvature value and vice versa. In other words, a mean curvature of zero indictates that the saddle surface shows the same magnitude of curvature in both directions.

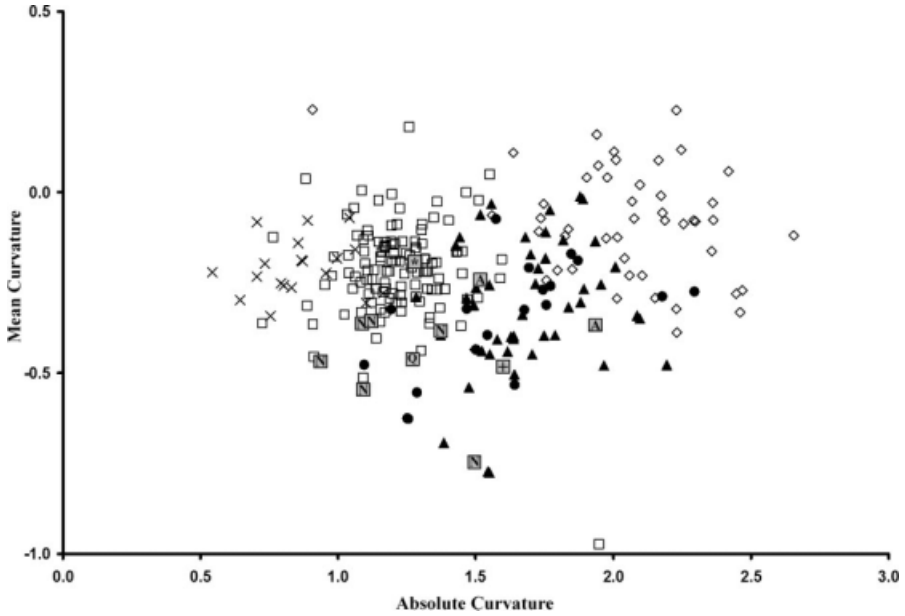

Fig. 11. Bivariate plot showing the relation between absolute and mean curvatures of the surface on the metacarpal (symbols as in Fig. 7). Greater values of absolute curvature indicate greater overall surface curvature; mean curvature values closer to zero indicate more evenly curved surfaces, while negative values indicate radioulnar curvature is greater than dorsovolar curvature (and vice versa).

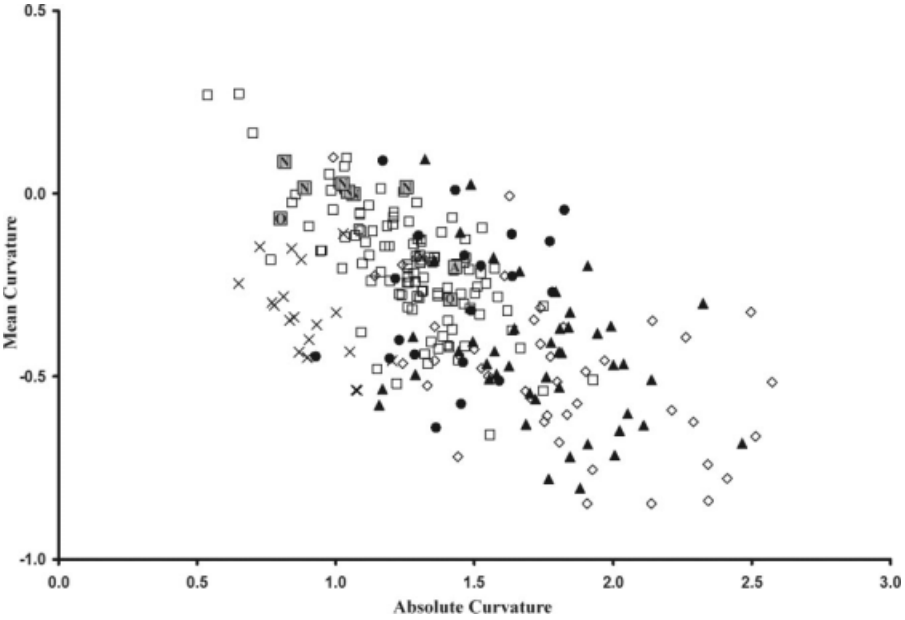

Fig. 12. Bivariate plot showing the relation between absolute and mean curvatures of the surface on the trapezium (symbols as in Fig. 8). Greater values of absolute curvature indicate greater overall surface curvature; mean curvature values closer to zero indicate more evenly curved surfaces, whereas negative values indicate dorsovolar curvature is greater than radioulnar curvature (and vice versa).

The joint congruence indices (Table 5) indicate significantly greater RMS and radioulnar congruence of the joint surfaces in *Homo* than in the great apes and *Papio*. The human joint in our sample is more congruent in the radioulnar than in the dorsovolar direction, as Napier (1955) and Ateshian et al. (1992) also found for humans. *Pan* similarly is more congruent in the radioulnar direction, but is striking in its very marked dorsovolar incongruence.

Comparison of fossil hominins with the extant sample

Analyses of SPG and LS data for the early hominin fossils have similar results (Table 6). There is a tendency toward greater RMS curvature of the mutual tmc surfaces in *A. afarensis* compared with humans and much lower RMS curvature of the O.H. 7 trapezial surface (see

Table 3). In the SPG analysis, the A.L. 333-w39 metacarpal surface RMS curvature (1.59) falls close to the chimpanzee mean (1.62), and the A.L. 333-80 trapezial surface is coincident with the chimpanzee mean (1.85). LS places the metacarpal (1.13) more than one SD unit below the chimpanzee RMS mean (1.29) and more than 1 SD unit above the human mean (0.93). However, the LS value for the other *A. afarensis* metacarpal, A.L. 333-58 (1.46), is more than four SD units higher than the human mean (0.93) and close to the gorilla mean (1.47). The LS dorsovolar curvatures of the *A. afarensis* metacarpal and trapezial surfaces differ in the same general directions as the RMS curvatures (Figs. 7 and 8). Radioulnar curvature follows similar trends, but A.L. 333-58 shows higher curvature than the means of the living hominids[2], and a similar result is observed for radioulnar curvature of the A.L. 333-80 trapezium.

RMS curvature of the SK 84 metacarpal surface (Table 6) is near the *Pan* mean, although the dorsovolar and radioulnar curvatures result in this fossil clustering toward one end of the *Pan* range of variation (see Fig. 9). The dorsovolar value is below the means of humans and all the great ape genera while radioulnar curvature is higher than the means of all the living genera and quite similar to that of A.L. 333-58. In contrast, all the SKX 5020 curvature values are close to those of *Homo*, and the metacarpal falls well within the modern human cluster (see Fig. 9). It should be noted that there is not agreement regarding the affinities of either the SK 84 or the SKX 5020 specimens (see Susman, 1988a; Trinkaus and Long, 1990; Tocheri et al., 2008).

In contrast to *A. afarensis*, the *H. habilis* O.H. 7 trapezial SPG mean RMS curvature is one SD below the SPG human mean, and the LS mean is outside the means of all genera, including *Papio* (see Fig. 10). Dorsovolar curvature is also below all LS sample means, whereas radioulnar curvature is below that of all LS genera except *Papio* (see Fig. 8).

The Neandertal tmc surfaces are typically flatter dorsovolarly than in most of the modern human sample (Table 6; Figs. 7 and 8) with radioulnar curvature values that fall within the modern human range. Several Neandertals display RMS curvatures of the metacarpal surface close to the modern human mean (see Fig. 9), whereas the Neandertal trapezial RMS and dorsovolar curvatures fall toward one end of the modern human range (Figs. 8 and 10), recalling the condition seen in O.H. 7. However, the high-radioulnar curvature distinguishes the Neandertals from *H. habilis* (see Fig. 8).

DISCUSSION

Curvature variability

No predictions were falsified by the analysis. Human tmc joint surfaces are less curved than in the great apes in all directions. The only exception is trapezial radioulnar curvature, which is approximately the same in all the hominids. Neandertal dorsovolar and O.H. 7 dorsovolar and radioulnar curvatures are lower than in modern humans, australopith curvatures recall those of African apes, and the two Swartkrans metacarpals differ in curvature as predicted.

[2]See footnote 1.

TABLE 5. Congruence indices[1]

Genus	Dorsovolar	Radioulnar	RMS
a. *Homo*	0.44^{b}	0.39^{ALL}	0.29^{ALL}
b. *Pan*	0.81^{ALL}	$0.74^{a,e}$	$0.55^{a,c,e}$
c. *Gorilla*	0.43^{b}	$0.70^{a,e}$	$0.41^{a,b}$
d. *Pongo*	0.53^{b}	0.71^{a}	0.44^{a}
e. *Papio*	0.57^{b}	$0.55^{a,b,c}$	$0.40^{a,b}$

[1] Superscripts indicate significant differences among genera a–e at $\alpha < 0.0025$.

Implications of curvature variability for joint mobility, strength and stability

Joint mobility. Hamrick (1996) found an association between high male joint mating surface curvature and increased joint mobility in carpal joints of strepsirhine primates. In contrast, our study shows higher trapezial dorsovolar curvature and higher metacarpal radioulnar curvature in great apes compared with humans, but there is a lower range of motion in both directions in great apes according to Rose (1992). As Hamrick (1996) noted, conclusions from his analysis may not apply to different joint types, movements, and taxa, and in our study, this appears to be the case at least for hominids. Humans share with the other genera a metacarpal male surface for radioulnar deviation associated with a less-curved female trapezial surface. This pattern may suggest a potential for considerable mobility in this plane, as suggested by Hamrick (1996) for strepsirhine carpal movements. However, variation among the genera in joint congruence must be taken into account in assessing full potential ranges of motion.

Joint strength. Human RMS and dorsovolar curvatures of the trapezium and metacarpal are lower than those of the great apes, providing more surface normal to axial loads. In addition, humans have greater RMS and radioulnar congruence of the mutual tmc joint surface curvatures than the great apes. This pattern is favorable to accommodation of the large axial loads associated with forceful pinch and grasp of objects.

Cartilage thickness, joint shape, and subchondral bone may be sensitive to loading history (Carter and Beaupré, 2001). It would be interesting to compare humans with nonhuman primates in tmc subarticular trabecular bone properties, because these have been found by Rafferty and Ruff (1994) in the humeral and femoral heads and by Patel and Carlson (2007) at the distal radius to correspond to differences in magnitude of loads.

Joint stability. The greater dorsovolar curvature of the African ape metacarpal surface creates a long volar beak. Attempts to slide the metacarpal dorsally on the trapezium in cadaver and skeletal specimens are resisted by abutment of the beak against the convex volar trapezial surface. Lower curvature in humans is associated with a less-projecting beak and less stability of the joint. The shallower human joint has the advantage of accommodating relatively more axial load, but at the potential expense of resistance to dorsal subluxation of the metacarpal at tmc joints with lax ligaments, when objects are pinched by the thumb and index finger (Pellegrini et al., 1993; Pellegrini, 2001).

Noteworthy is the exceptionally high-dorsovolar curvature of the trapezium and metacarpal in the gorillas, reflected also in their high RMS and Gaussian curvatures. In addition, the joint is the most dorsovolarly con-

TABLE 6. Normalized trapeziometacarpal joint surface curvature values in hominin fossils

Specimen	Approach	Joint surface	RMS	Dorsovolar	Radioulnar	Absolute	Gaussian	Mean
A.L. 333w-39	SPG	Metacarpal	1.59					
	LS		1.13	0.52	−1.0	1.52	−0.52	−0.24
A.L. 333-58	LS	Metacarpal	1.46	0.60	−1.34	1.94	−0.8	−0.37
A.L. 333-80	SPG	Trapezium	1.85					
	LS		1.05	−0.92	0.51	1.43	−0.47	−0.2
O.H.7	SPG	Trapezium	1.09					
	LS		0.57	−0.47	0.33	0.80	−0.16	−0.07
SKX 5020	LS	Metacarpal	0.94	0.44	−0.83	1.28	−0.37	−0.19
SK 84	LS	Metacarpal	1.32	0.32	−1.28	1.6	−0.41	−0.48
Kebara 2	LS	Metacarpal	1.08	−0.01	−1.08	1.09	0.01	−0.55
Kebara 2	LS	Trapezium	0.63	−0.43	0.46	0.89	−0.2	0.02
La Ferrassie 1	LS	Metacarpal	0.94	0.2	−0.92	1.12	−0.19	−0.36
La Ferrassie 1	LS	Trapezium	0.75	−0.54	0.53	1.07	−0.28	0.0
La Ferrassie 2	LS	Metacarpal	1.11	0.3	−1.07	1.37	−0.32	−0.38
La Ferrassie 2	LS	Trapezium	0.89	−0.61	0.65	1.26	−0.39	0.02
Regourdou 1	LS	Metacarpal	0.87	−0.07	−0.87	0.94	0.06	−0.47
Regourdou 1	LS	Trapezium	0.74	−0.52	0.53	1.04	−0.27	0.0
Amud 1	LS	Metacarpal	0.93	0.18	−0.91	1.09	−0.16	−0.36
La Chapelle 1	LS	Metacarpal	1.18	−0.38	−1.12	1.49	0.42	−0.75
Shanidar 3	LS	Trapezium	0.73	−0.49	0.54	1.02	−0.26	0.03
Shanidar 4	LS	Trapezium	0.59	−0.32	0.49	0.82	−0.16	0.09

gruent of the great ape genera. This pattern, favoring tmc joint stability, should be investigated in connection with the forceful pulling and processing of vegetation by gorillas observed in videotapes taken by R. Byrne [cited by Marzke (2006)].

The baboons are clearly distinguished from the hominid sample by the low curvature of the mutual joint surfaces in the dorsovolar direction, and even lower values in the radioulnar direction. This latter feature often gives the joint an almost cylindrical appearance, particularly on the trapezial surface. Low RMS and absolute curvature values all indicate relatively flat surfaces in the baboons, but negative Gaussian curvature values lend support to the conclusions of Napier (1961), Lewis (1977), and Rose (1992) that baboons have saddle surfaces, albeit shallow ones. Furthermore, our low baboon radioulnar curvature values confirm the observations by Rose (1992) that cercopithecines differ most clearly from hominoids in radioulnar curvature and associated abduction range. He suggests that the lower range in the cercopithecines might limit grasp of relatively large objects and affect opposition of the thumb to the fingers, because abduction is an important component of thumb opposition. Also, because opposition of the thumb metacarpal appears to occur without obvious constraints on displacement of the metacarpal from the trapezium, this may explain the observations of Guthrie (1991) and Jude (1993) that manipulation of objects by Hamadryas baboons does not involve the kinds of strong pinch and grasp forces that would tend to displace the metacarpal.

Phylogenetic implications of the comparative joint curvature evidence

The results of this study present compelling evidence that the overall pattern of metacarpal and trapezial surface curvature is derived in humans relative to their last common ancestor with *Pan*. Although humans approach baboons in magnitude of curvature more closely than do the great apes, the topographic pattern is different. The baboon surfaces are almost flat in the radioulnar direction, and only slightly more curved in the dorsovolar direction, forming a pattern that approaches a cylinder in shape (Figs. 7 and 8). The human saddle-shaped pattern more strongly recalls the great ape saddle, differing primarily in the magnitude of curvature rather than in overall shape. The cylinderlike morphology in baboons, with metacarpal movement occurring primarily in flexion/extension around the radioulnar axis, may underlie differences in joint biomechanics and functional capabilities that should be investigated.

Evolution of modern human tmc joint functions and manipulative behavioral capabilities

The australopiths recall African apes most strongly in RMS and dorsovolar curvatures, indicating a joint that was stable against dorsal displacement in thumb/index finger pinch grips and capable of accommodating stresses from several directions. It is interesting to note that while these australopiths also share curved phalanges with the great apes, suggestive of arboreal locomotor capabilities (Stern, 2000), and proportionately short fingers relative to thumb length (Alba et al., 2003) recalling humans, they differ from both in having more radioulnar curvature at the tmc joint (Figs. 7 and 8). This combination of features suggests locomotor and manipulative behaviors that may have differed to some extent from those of both living great apes and humans.

The earliest evidence for reduction in tmc curvature is in one of two Swartkrans thumb metacarpals (SKX 5020), and in the O.H. 7 trapezium, both from ~1.75 mya (Vrba, 1982; Walter et al., 1991; Blumenschine et al., 2003). The SKX 5020 curvature falls within the modern human range of variation, whereas the O.H. 7 trapezium has a significantly flatter joint surface overall than modern humans. This morphology suggests that the trapezium could have accommodated large axial loads, as predicted by Trinkaus (1989). Neandertals are similar to the O.H. 7 hominin in dorsovolar flatness of the joint; however, they display radioulnar curvature values within the modern human range. As Niewoehner (2000, 2001) noted, the primary shape change at the Neandertal tmc joint is the low degree of metacarpal volar beak development, from which he infers an adaptation to large axial reaction forces. It is likely that the joint was

relatively unstable in both Neandertals and O.H. 7 in comparison with modern humans, in the absence of a projecting metacarpal beak to check dorsal subluxation with pinch by the thumb and index finger. Stability would have depended upon the tmc ligaments.

Modern human tmc joint topography appears to be a morphological compromise: it is flat enough to allow accommodation of large axial forces associated with forceful manipulative gripping, but curved enough to resist subluxation in strong pinch (if the ligamentous apparatus is intact). Biomechanical experiments and examination of diseased human tmc joints have shown that initial cartilage destruction at the joint occurs near the attachment of the beak ligament and is accompanied by degeneration of the ligament (Pellegrini, 2005). The more curved African ape-like ancestral hominin joint would have been vulnerable to stress as prehistoric toolmaking and tool-using behaviors focused increasingly large axial and shear stresses on the joint with forceful precision and power squeeze grips. Thus, the evolutionary reduction of metacarpal surface curvature and shortening of the volar metacarpal beak may have been advantageous as hominins became more dependent on tool-related behaviors for survival.

The loss of ancestral morphology in favor of derived morphology that likely has performance advantages for object manipulation may reflect an evolutionary commitment to behaviors involving tool making and tool use that occurred in the hominin lineage leading to modern humans and Neandertals (Tocheri, 2007; Tocheri et al., 2007, 2008). The clinical prevalence today of osteoarthritis at joint contact points stressed by forceful manipulative grips and of metacarpal subluxation associated with habitual forceful thumb/index finger pinching of objects, noted earlier in the section on joint stability, is suggestive of the kinds of functional liabilities that may have channeled the evolution of hand joint structure during hominin cultural and morphological evolution.

ACKNOWLEDGMENTS

We thank L. Berglund, Mayo Clinic Orthopedic Biomechanics Laboratory, for his help in the development of our system for photographing the specimens. Equipment and software for laser scanning and quadric surface analysis were provided by the Partnership for Research in Spatial Analysis (PRISM) at ASU. Special thanks to A. Razdan and G. Farin (ASU) for encouraging the development of this research. Access to specimens was kindly provided by D. Hunt, R. Potts, L. Gordon, and R. Thorington (NMNH), B. Latimer and L. Jellema (CNH), E. Trinkaus (WUSTL), and W. Kimbel and D. Johanson (IHO-ASU). We are also grateful to the Primate Foundation of Arizona for access to their chimpanzee skeletal collection. C. Linscheid, K. Stotesbury, and A. de Sousa provided invaluable assistance in data collection and digitization.

LITERATURE CITED

Alba DM, Moya-Sola S, Kohler M. 2003. Morphological affinities of the *Australopithecus* hand on the basis of manual proportions and relative thumb length. J Hum Evol 44:225–254.

Ateshian GA, Ark JW, Rosenwasser MP, Pawluk RJ, Soslowsky LJ, Mow VC. 1995. Contact areas in the thumb carpometacarpal joint. J Orthop Res 13:450–458.

Ateshian GA, Kwak S, Soslowsky LJ, Mow VC. 1994. A stereophotogrammetric method for determining *in situ* contact areas in diarthroidial joints, and a comparison with other methods. J Biomech 27:111–124.

Ateshian GA, Rosenwasser MP, Mow VC. 1992. Curvature characteristics and congruence of the thumb carpometacarpal joint: differences between female and male joints. J Biomech 25:591–607.

Bettinger PC, Berger RA. 2001. Functional ligamentous anatomy of the trapezium and trapeziometacarpal joint (gross and arthroscopic). Hand Clin 17:151–168.

Bettinger PC, Linscheid RL, Berger RA, Cooney WP III, An K-N. 1999. An anatomic study of the stabilizing ligaments of the trapezium and trapeziometacarpal joint. J Hand Surg A 24:786–798.

Bettinger PC, Smutz P, Linscheid RL, Cooney WP III, An K-N. 2000. Material properties of the trapezial and trapeziometacarpal ligaments. J Hand Surg A 25:1085–1095.

Blumenschine RJ, Peters CR, Masao FT, Clarke RJ, Deino AL, Hay RL, Swisher CC, Stanistreet IG, Ashley GM, McHenry LJ, Sikes NE, van der Merwe NJ, Tactikos JC, Cushing AE, Deocampo DM, Njau JK, Ebert JI. 2003. Late Pliocene *Homo* and hominid land use from Western Olduvai Gorge. Tanzania. Science 299:1217–1221.

Brand PW, Hollister AM. 1999. Clinical mechanics of the hand, 3rd ed. Mosby: St. Louis.

Bruce P, Simon J, Oswald T. 1997. Resampling stats users guide. Arlington: Resampling Stats.

Carter DR, Beaupré GS. 2001. Skeletal function and form. Cambridge: Cambridge University Press.

Cerveri P, De Momi E, Marchente M, Lopomo N, Baud-Bovy G, Barros RML, Ferrigno G. 2008. In vivo validation of a realistic kinematic model for the trapezio-metacarpal joint using an optoelectronic system. Ann Biomed Eng 36:1268–1280.

Christie PW, Ridley JN. 1990. Classification and mathematical representation of synovial articular surfaces. In: Sperber GH, editor. From Apes to angels: essays in Anthropology in honor of Philip V. Tobias. New York: Wiley-Liss. p 111–117.

Colman M, Mass DP, Draganich LF. 2007. Effects of the deep anterior oblique and dorsoradial ligaments on trapeziometacarpal joint stability. J Hand Surg A 32:310–317.

Cooney WP III, Chao EYS. 1977. Biomechanical analysis of static forces in the thumb during hand function. J Bone Joint Surg Am 59:27–36.

Cooney WP III, Lucca MJ, Chao EYS, Linscheid RL. 1981. The kinesiology of the thumb trapeziometacarpal joint. J Bone Joint Surg A 63:1371–1381.

Day MH. 1978. Functional interpretations of the morphology of postcranial remains of early African hominids. In: Jolly CJ, editor. Early hominids of Africa. London: Gerald Duckworth & Company Ltd. p 311–345.

Eaton RG, Dray GJ. 1982. Dislocations and ligament injuries in the digits. In: Green DP, editor. Operative hand surgery, Vol. 1. New York: Churchill. p 637–668.

Edgington E. 1995. Randomization tests. New York: Marcel Dekker.

Efron B, Tibshiriani RJ. 1993. An introduction to the bootstrap. Boca Raton, FL: CRC Press.

Guthrie EA. 1991. Variability of the primate trapeziometacarpal articulation: description and functional evolution significance, M.A. thesis, Arizona State University, Arizona.

Hamrick MW. 1996. Articular size and curvature as determinants of carpal joint mobility and stability in strepsirhine primates. J Morph 230:113–127.

Hollister A, Buford W, Myers L. 1992. Axes of rotation of the thumb carpometacarpal joint. J Orthop Res 10:454–460.

Imaeda T, Niebur G, Cooney WP III, Linscheid RL, An K-N. 1994. Kinematics of the normal trapeziometacarpal joint. J Orthop Res 12:197–204.

Jude J. 1993. Manipulative behavior of hamadryas baboons, Senior thesis, Arizona State University, Arizona.

Koff MF, Shrivastava N, Gardner TR, Rosenwasser MP, Mow VC, Strauch RJ. 2006. An *in vitro* analysis of ligament reconstruction or extension osteotomy on trapeziometacarpal joint stability and contact area. J Hand Surg A 31:429–439.

Leakey LSB. 1960. Recent discoveries at Olduvai Gorge. Nature 188:1050–1052.
Leakey LSB, Tobias PV, Napier JR. 1964. A new species of the genus *Homo* from Olduvai Gorge. Nature 202:7–9.
Leversedge FJ. 2008. Anatomy and pathomechanics of the thumb. Hand Clin 24:219–229.
Lewis OJ. 1977. Joint remodeling and the evolution of the human hand. J Anat 123:157–201.
Lewis OJ. 1989. Functional morphology of the evolving hand and foot. Oxford: Clarendon Press.
Manly BFJ. 1997. Randomization, bootstrap and Monte Carlo methods in biology, 2nd edition. Boca Raton, FL: CRC Press.
Martin RB, Burr, DB, Sharkey NA. 1998. Skeletal tissue mechanics. New York: Springer-Verlag.
Marzke MW. 2006. Who made stone tools? In: Roux V, Bril B, editors. Stone knapping: the necessary conditions for a uniquely hominin behaviour. University of Cambridge, Cambridge: McDonald Institute for Archaeological Research. p 243–255.
Marzke MW, Wullstein KL. 1996. Chimpanzee and human grips: a new classification with a focus on evolutionary morphology. Int J Primatol 17:117–139.
Momose T, Nakatsuchi Y, Saitoh S. 1999. Contact area of the trapeziometacarpal joint. J Hand Surg A 24:491–495.
Mooney CZ, Duval RE. 1993. Bootstrapping. Newbury Park: Sage.
Napier JR. 1955. The form and function of the carpo-metacarpal joint of the thumb. J Anat 89:362–369.
Napier JR. 1961. Prehensility and opposability in the hands of primates. Symp Zool Soc Lond 5:115–132.
Napier JR. 1962. Fossil hand bones from Olduvai Gorge. Nature 196:409–411.
Niewoehner WA. 2000. The functional anatomy of Late Pleistocene and recent human carpometacarpal and metacarpophalangeal articulations, Ph.D. dissertation, University of New Mexico, New Mexico.
Niewoehner WA. 2001. Behavioral inferences from the Skhul/Qafzeh early modern human hand remains. PNAS 98:2979–2984.
Patel BA, Carlson KJ. 2007. Bone density spatial patterns in the distal radius reflect habitual hand postures adopted by quadrupedal primates. J Hum Evol 52:130–141.
Pellegrini VD Jr. 2001. Pathomechanics of the thumb trapeziometacarpal joint. Hand Clin 17:175–184, vii-viii.
Pellegrini VD Jr. 2005. The ABJS. 2005. Nicolas Andry Award: osteoarthritis and injury at the base of the human thumb: survival of the fittest? Clin Orthop Relat Res 438:266–276.
Pellegrini VD Jr, Olcott CW, Hollenberg G. 1993. Contact patterns in the trapeziometacarpal joint: the role of the palmar beak ligament. J Hand Surg A 18:238–244.
Pieron AP. 1973. The mechanism of the first carpometacarpal (CMC) joint. An anatomical and mechanical analysis. Acta Orthop Scand Suppl 148:1–104.
Rafferty KL, Ruff CB. 1994. Articular structure and function in *Holobates, Colobus,* and *Papio*. Am J Phys Anthropol 94:395–408.
Rose ME. 1992. Kinematics of the trapezium-1st metacarpal joint in extant anthropoids and Miocene hominoids. J Hum Evol 22:255–266.
Sarmiento EE. 1988. Anatomy of the hominoid wrist joint: its evolutionary and functional implications. Int J Primatol 9:281–345.
Simon JL. 1974–1997. Resampling stats: the new statistics, Version 4.0.7. Resampling Stats Inc.
Steinberg B. 1999. The use of B-spline sufaces for modeling and analysis of bone shapes, M.S. thesis, Arizona State University, Arizona.
Stern JT. 2000. Climbing to the top: a personal memoir of *Australopithecus afarensis*. Evol Anthropol 9:113–133.
Susman RL. 1998a. Hand of *Paranthropus robustus* from Member 1. Swartkrans: fossil evidence for tool behavior. Science 240:781–784.
Susman RL. 1988b. New postcranial remains from Swartkrans and their bearing on the functional morphology and behavior of *Paranthropus robustus*. In: Grine FE, editor. Evolutionary history of the "Robust" Australopithecines. New York: Aldine de Gruyter. p 149–172.
Susman RL, Creel N. 1979. Functional and morphological affinities of the subadult hand (OH 7) from Olduvai Gorge. Am J Phys Anthropol 51:311–331.
Tocheri MW. 2007. Three-dimensional riddles of the radial wrist: derived carpal and carpometacarpal joint morphology in the genus *Homo* and the implications for understanding stone tool-related behaviors in hominins, Ph.D. dissertation, Arizona State University, Arizona.
Tocheri MW, Femiani JC. In press. The "bare bones" of 3D: an introduction to 3D modeling concepts for the physical anthropologist. In: Hoppa RD, Nelson AJ, editors. 3D imaging in biological anthropology and bioarchaeology. Cambridge: Cambridge University Press.
Tocheri MW, Femiani J, Orr CM, Marzke MW. 2006. Quadric-based metrics for shape analysis of three-dimensional osteological surfaces. Am J Phys Anthropol 129:177–178.
Tocheri MW, Orr CM, Jacofsky MC, Marzke MW. 2008. The evolutionary history of the hominin hand since the last common ancestor of *Pan* and *Homo*. J Anat 212:544–562.
Tocheri MW, Orr CM, Larson SG, Sutikna T, Jatmiko, Saptomo EW, Awe Due R, Djubiantono T, Morwood MJ, Jungers WL. 2007. The primitive wrist of *Homo* floresiensis and its implications for hominin evolution. Science 317:1743–1745.
Trinkaus E. 1989. Olduvai hominid 7 trapezial metacarpal 1 articular morphology: contrasts with recent humans. Am J Phys Anthropol 80:411–416.
Trinkaus E, Long JC. 1990. Species attribution of the Swartkrans Member 1 first metacarpals: SK 84 and SKX 5020. Am J Phys Anthropol 83:419–424.
Vrba ES. 1982. Biostratigraphy and chronology, based particularly on Bovidae, of southern hominid-asociated assemblages: Makapansgat, Sterkfontein, Taung, Kromdraai, Swartkrans; and also Elandsfontein (Saldanha), Broken Hill (now Kabwe) and Cave of Hearths. In: DeLumley F, DeLumley MA, editors. L'*Homo erectus* et la place de l'homme de Tautavel parmi les hominidés fossils. Prétirage du 1er congrès international paléontologie humaine, Vol. 2. Nice: Louis-Jean. p 707–752.
Walter RC, Manega PC, Hay RL, Drake RE, Curtis GH. 1991. Laser-fusion $^{40}Ar/^{39}Ar$ dating of Bed I. Olduvai Gorge, Tanzania. Nature 354:145–149.
Wood B, Lonergan N. 2008. The hominin fossil record: taxa, grades and clades. J Anat 212:354–376.
Xu L, Stauch RJ, Ateshian GA, Pawluk RJ, Mow VC, Rosenwasser MP. 1998. Topography of the osteoarthritic thumb carpometacarpal joint and its variations with regard to gender, age, site, and osteoarthritic stage. J Hand Surg A 23:454–464.